ISSN PRINT 2319 1775 Online 2320 7876

 UGC CARE Listed (Group -I) Journal Volume 11 , Iss 8, Aug 2022

Internal Combustion Engine Air-Fuel Ratio Management Utilising an Artificial Neural Network with Sliding Mode Control Designed to Tolerate Sensor Failures

U.Dinesh Kumar[1], M.Ganga Pavan Kumar[2]

[1,2]Assistant Professor, Department Of Mechanical Engineering,CVRT Engineering college, Tadipatri

ABSTRACT

Using artificial neural networks (ANNs) and sliding mode controls (SMCs) for the active and passive components, respectively, this research offers a new hybrid fault-tolerant control system (HFTCS). The suggested system has the potential to provide both post-fault optimum performance and stability against unanticipated quick disturbances. The observer model of an active fault tolerant control system (AFTCS) includes a fault detection and isolation (FDI) unit that estimates bad sensor data using an artificial neural network (ANN). A robust state-machine controller (SMC) is used to construct the air-to-fuel ratio (AFR) controller in the PFTCS component, which enables for fault management within specified bounds without the need for estimate. SMC will be the passive component that responds immediately to faults, while ANN will be the active component that optimises performance post-fault via active compensation. In addition, a Lyapunov stability study was carried out to guarantee the system's steadiness under both typical and abnormal operating settings. The Matlab/Simulink simulation results demonstrate that the suggested controller can withstand errors in both clean and noisy sensor measurements. When compared to prior efforts, the proposed hybrid algorithm is shown to have greater performance.

KEYWORDS: Artificial neural network, sliding mode control, air-fuel ratio control, Lyapunov stability, and fault-tolerant control.

1. INTRODUCTION

Fault-tolerant control systems (FTCS) are regarded as modern control systems to achieve higher reliability and stability. A fault is classified as a deviation from the standard operating value of a plant parameter. Faults in a system can jeopardize the desired operation of the whole system. An FTCS may work under faulty conditions and stay stable; however, performance loss can occur. The FTCS may also be used to maintain stability because of the safety of people, and missionsensitive applications like aircraft, and unmanned air vehicles (UAVs).1–3 Due to variations in architectures and properties, FTCS is divided into two major cate- gories: active and passive. Some symbols and abbrevia- tions related to HFTCS are listed in Tables 1 and 2, respectively.

ISSN PRINT 2319 1775 Online 2320 7876

 UGC CARE Listed (Group -I) Journal Volume 11 , Iss 8, Aug 2022

Table 1. List of abbreviations.

Abbreviation	Explanation
FTC	Fault-tolerant control
HFTCS	Hybrid fault-tolerant control system
PFTCS	Passive fault-tolerant control system
AFTCS	Active fault-tolerant control system
SMC	Sliding mode control
ANN	Artificial neural network
AFR	Air-fuel ratio
AR	Analytical redundancy
IC Engine	Internal combustion engine
MVEM	Mean value engine model
MAP	Manifold air pressure.
EGO	Exhaust gas oxygen sensor

Table 2. List of symbols.

Symbol	Explanation
m_{air}	Mass of air
m_{fuel}	Mass of fuel
T_{in}	Input temperature
P_{in}	Manifold pressure
v_{in}	Input volume
$\dot{m}_{th}$	Mass flow through the valve
$\dot{m}_{Cyl}$	Mass flow into cylinders
R	Gas constant
N_e	Engine speed
e_x	Residual
ϕ_{th}	Throttle opening position
C_d	Discharge coefficient
$S_{es}(\phi_{th})$	True throttle opening position
γ	Heat-ratio of air
τ_f	Fuel vapor process
$\dot{m}_{fi}(t)$	Fuel flow injection
$\dot{m}_f(t)$	Fuel flow into cylinders
$\dot{m}_{fv}$	Vapor fuel flow
$\dot{m}_{fl}(t)$	Liquid mass fuel flow
$\lambda(t)$	Lambda sensor
τ_λ	Time delay
y_d	Desired output
y	Actual output
u	Actual Input
x_1/x_2	State variables
α/β	Parameters of engine
$\hat{x}_1/\hat{x}_2$	Estimated values of observer design
$\hat{y}$	Estimated output
E	Root mean square error
η	Learning rate
$\Xi_i(x)$	Base function
Δ_i	Unknown constant parameter
S_{oi}	Conventional sliding mode design
U_o	Maintain the known terms
M_i	Unstructured uncertainties
Θ_i	Structured faults
Θ_1 and Θ_2	Over and underflow

In active fault-tolerant system (AFTCS), the fault detection and isolation (FDI) unit is designed to detect the fault in the online mode and it isolates faulty val- ues.4–6 The FDI unit compares the values of the actual sensors with the estimated values being generated from the observer for a residual generation. The fault in the component is declared when the residual value exceeds its predefined limiting value. The controller is then reconfigured to adapt according to the current faulty conditions after fault detection and isolation, with little output deterioration.7,8 Unlike AFTCS, passive fault- tolerant system (PFTCS) may not need a dedicated FDI unit, and any fault in the design stage of the con- trol system is considered beforehand in the offline mode.9–11 PFTCS is, therefore, very swift than AFTCS due to lesser computational cost, but it has the draw- back to deal with the faults only that were

ISSN PRINT 2319 1775 Online 2320 7876

Research paper **© 2012 IJFANS. All Rights Reserved, UGC CARE Listed (Group -I) Journal Volume 11 , Iss 8, Aug 2022**

considered during the construction of the controller.12,13 A combi- nation of all these approaches is also built by integrat- ing both types, namely hybrid fault-tolerant control system (HFTCS). In protective and safety applications, the hybrid system can rapidly respond to faults with the PFTCS property and later optimize itself with the AFTCS property.14–16 In Amin,14 the HFTCS has been proposed with Kalman Filters in the active part and a high-gain PI controller in the passive part. This algo- rithm was limited to the linear range of the highly non- linear sensors of the AFR control system. In Su et al.,15 the HFTCS was proposed for the sensors of the distilla- tion column without using any intelligent control or data-driven technique. In Wang et al.,16 the HFTCS was proposed for the uncertain networked control sys- tems under a discrete event-triggered communication scheme that was not applied to the process plant.

A comprehensive study of the FTCS has been men- tioned for the nonlinear system in Li17 for various fault scenarios. In Yang et al.,18 the non-linear hybrid FTCS design was established for feature extraction, and the actuator fault adjustment control was applied. The arti- ficial neural networks (ANN) technique was applied for the switched-type nonlinear systems in Tang et al..19 For a single-tank system with system faults and process disturbances, a fuzzy logic-based passive fault-tolerant control method was proposed in Patel and Shah.20 In Murtaza et al.,21 a super-twisting control-based unified FDI and FTC system for the air path of diesel engines is reported. Kalman Filters (KFs) were also used in the FDI architecture of gas turbines for faulty sensor esti- mation22,23 consisting of both hardware and analytical redundancies.

Artificial neural networks

The artificial neural network (ANN) includes the con- cept of artificial intelligence, whose aim is to allow the systems to learn from experience. ANN works on the same logic as a human brain. It is a smart and modern approach to data-driven problems.24 This non-linear technique is used in real-time problems like the model- ing of the engine because the engine is a highly non- linear system and ANN provides an optimal solution for such highly nonlinear problems.25–27 The architec- ture of the ANN is shown in Figure 1.

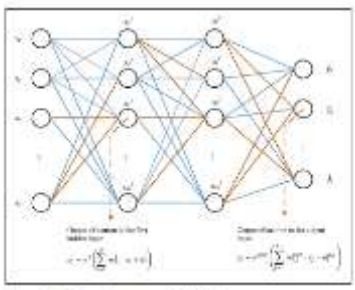

Figure 1. The architecture of ANN.[24]

ANN performs a data-parallel function, therefore, sequential simulations are easier than standard systems. The ANN works with both forward and backpropaga- tion. Its multi-layer perceptron model is known as a backpropagation neural network (BPNN).28–30 The input is in the form of samples and is treated with dif- ferent multiple hidden layers before the required output is mapped through this input. In Gao et al.,30 FTC architecture was proposed with an adaptive neural net- work for Multi-Input Multi-Output (MIMO) systems. In Wang et

ISSN PRINT 2319 1775 Online 2320 7876

Research paper **© 2012 IJFANS. All Rights Reserved,** UGC CARE Listed (Group -I) Journal Volume 11 , Iss 8, Aug 2022

al.,31 the ANN is utilized with a backpropa- gation strategy for the fault-tolerant control system. An adaptive neural network for the unmolded dynamic solution is proposed in Yin et al.32 The dataset is mapped to real numbers, that is, (x, y) where x repre- sents the selected feature and y translates the health state to this feature. ANN is described in terms of mathematical form is,

$$a_j^l = \sigma \sum_k w_{jk}^l a_k^{l-1} + b_j^l \qquad (1)$$

where wl represents the weight matrix inputs, bl shows the bias vector for layers l, and al is activation vector with the activation elements al.

Sliding mode control

Robust control is a control system architecture tech- nique that can allow systems to manage faults as long as the faults stay within the predefined limits.33,34 Robust control systems are static rather than dynamic and do not adjust to their conditions. For example, a high-gain feedback system is a robust control system due to its high gain, and changes in the other para- meters prove negligible due to its robustness. Sliding mode control (SMC) is derived from a variable struc- ture control system that mostly incorporates various control structure features and performs better than existing classical control structures.35,36 There are two phases in the SMC design as represented in Figure 2.

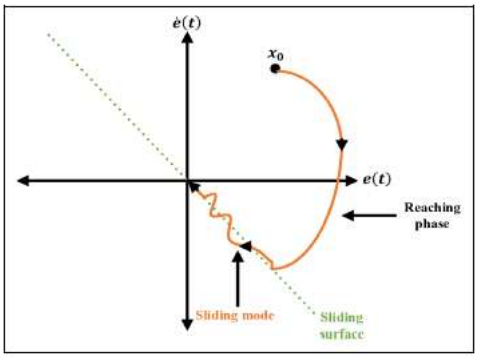

Figure 2. Sliding mode control.[33]

SMC triggers chattering in the actuator because of the rapid switching, therefore, a higher-order SMC named as super twisting algorithm is used to reduce the chattering problem.37 It is a non-linear technique with exceptional robustness properties. In practical terms, SMC facilitates non-linear processes that are subject to large model uncertainties. SMC will form the passive part in our proposed HFTCS to react instantly to faults.38

A customizable surface needs to be built in the first phase. The second phase should be planned to ensure that the system converges to the sliding surface for a minimum time. The phenomenon in which the motion takes place on a sliding surface is known as a sliding mode.38

AFR control of IC engines

The internal combustion engine is a type of heat engine in which the combustion of air and fuel takes place inside the cylinder and is used as the direct motive force. These engines transform the chemical energy of a fuel into thermal energy and use this energy to produce

ISSN PRINT 2319 1775 Online 2320 7876

Research paper **© 2012 IJFANS. All Rights Reserved,** UGC CARE Listed (Group -I) Journal Volume 11 , Iss 8, Aug 2022

mechanical work. Its two main types are known as Spark Ignition (SI) and Compression Ignition (CI). In SI engines, the combustion takes place with the help of spark plugs, while in CI engines, the heat of compres- sion is used for combustion.39

The term air-fuel ratio (AFR) is defined as a mixture ratio of proper fuel and air in the combustion chamber and it is widely used to enhance the reliability and effi- ciency of the IC engine. Its mathematical expression can be written as:

$$AFR = \frac{m_{air}}{m_{fuel}} \qquad (2)$$

where mair represents the mass of the air and mfuel rep- resents the mass of the fuel. The equation of AFR for gasoline mixture is,

$$25O_2 + 2C_8H_{18} \rightarrow 16CO_2 + 18H_2O + Energy \qquad (3)$$

According to this equation, AFR is said to be the stoi- chiometric ratio with a value of 14.6:1 for gasoline fuel and is desirable for optimum combustion, fuel energy savings, and reduced emissions levels. If the mixture has AFR greater than 14.6:1, it is known as a lean mix- ture with greater air than fuel. A mixture with lesser than 14.6:1 is termed a rich mixture with greater fuel than oxygen. However, both of them are considered to be harmful to the engine's performance and life as it decreases their efficiency. The value of AFR is different for various categories of fuels. For example, methanol values are 6.47:1, 9:1 for ethanol, and 34.3:1 for hydrogen.40

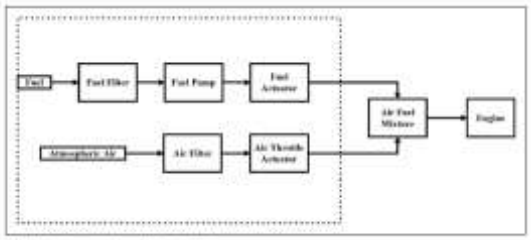

Figure 3. Air-fuel ratio control of an SI IC engine.[41]

The air-fuel mixing system of an SI IC engine is shown in Figure 3. Atmospheric air is filtered first and then passes through a throttle actuator. To change AFR more accurately by the AFR controller, the fuel actuator has been designed to adjust the fuel supply. The fuel is then first purified and transferred to the fuel actuator for flow control via the fuel pump. Air and fuel mixture is then made and provided for combustion to the engine cylinders. In the AFR control system of the IC engine, four sensors play an important role.

Throttle sensor: Often known as an air sensor. It provides the air throttle position signal to the engine control unit (ECU).

Manifold absolute pressure (MAP) sensor: It is also called a pressure sensor. It provides the suction manifold air pressure value to the ECU.

Speed sensor: It measures the speed of the engine crankshaft and provides to the ECU for controller calculations.

Exhaust gas oxygen (EGO) sensor: It's often referred to as a gas sensor. The concentration of oxygen in the exhaust of the IC engine is measured by an EGO sensor and provided to the ECU.

ISSN PRINT 2319 1775 Online 2320 7876

 UGC CARE Listed (Group -I) Journal Volume 11 , Iss 8, Aug 2022

In the paper, our contribution is to implement the novel HFTCS for the reliable operation of the IC engine to maintain the AFR in faulty conditions and prevent engine shutdown. In the proposed system, SMC will form the passive part to react instantly to faults while ANN will optimize post-fault performance with active compensation. Lyapunov stability analysis was performed to make sure that the system remains stable in both normal and faulty conditions. The fault tolerance is checked with noisy measurements of sen- sors to examine the robustness of the proposed control- ler. The simulation results in the Matlab/Simulink environment show that the designed controller is robust to faults in normal and noisy measurements of the sen- sors and reliable. Furthermore, the comparison with the existing works is carried out to demonstrate super- ior performance.
The structure of paper is organized as. Section ‘‘Research methodology’’ discusses the research metho- dology. Section ‘‘Results and discussions’’ presents the results and discussions. Section ‘‘Comparison with the existing works’’ elaborates on the comparison. Finally, the last section provides the conclusion of the paper.

Table 3. Model parameters.[41,42]

Parameters	Values
Engine speed	0–1000 rpm (300 rpm used in this study)
Throttle sensor range	0°–90°
MAP sensor range	0–1 bar
EGO sensor range	0–1 V
Specific heat ratio, γ	1.414

2. RESEARCH METHODOLOGY

The proposed HFTCS is implemented on the available IC engine model in Simulink. Mathworks explains preliminary knowledge and model working.41,42 In this model, the AFR system of the gasoline engine is built based on the findings of Crossley and Cook43 and was fully validated against dynamometer test data.42 The mathematical equations used for the model construction are in accordance with the mean value engine model (MVEM).44 Moreover, it gives accurate AFR as found in practical gasoline engines.40 HFTCS is a combination of AFTCS as well as PFTCS, as previously mentioned. AFTCS is designed using an ANN-based observer to build the FDI unit. In PFTCS, the AFR controller is designed using a robust SMC that allows systems to manage faults without many computations. The engine speed for this study is set at 300 r/min due to the design speed of the available MATLAB engine model. Therefore, a value of 300 is transmitted to the controller by the FDI unit in the case of a fault in the speed sensor. We utilized constant speed in this study since the engines in the process plant run at a constant speed most of the time, and the designed FDI provides the controller with 300 r/min of speed if the speed sensor fails. Because the paper is focused on designing an ANN-based AFTCS system, load changes and their impact on speed are not examined. The data for the MAP sensor and the throttle sensor at 300 r/min is derived using the available Matlab model lookup tables (LTs). To generate nonlinear interactions between the MAP sensor and the throttle sensor, the ANN approach is applied. For the generation of the estimated value of malfunctioning sensors, the

ISSN PRINT 2319 1775 Online 2320 7876

 UGC CARE Listed (Group -I) Journal Volume 11 , Iss 8, Aug 2022

FDI unit uses these nonlinear relationships. If the throttle and MAP sensors are faulty, the FDI unit generates an estimated value based on ANN observations and supplies to the ECU. The important parameters used in the model are mentioned in Table 3: First of all, the engine can work in its normal conditions if there is no fault. On the other hand, if a single sensor fault will happen, SMC will form the passive part to react instantly to faults while ANN will optimize post-fault performance with active compensation. Noise is introduced into the sensors, and their effect on the output is seen in normal as well as in faulty conditions to check the robustness of the proposed HFTCS. Zero seconds have been assumed when the sensors are switched. However, a delay possibly occurs in the switching actions. The limitations of the work are that only the full fault for sensors is carried out without taking partial faults which will be covered in future works. Engine AFR system modeling The modeling mentioned in this section is generic for complete theoretical analysis and adopted from well known literature.40,45 The control of the air-fuel ratio is divided into different dynamics: air dynamics, sensor model, and fuel dynamics. Air dynamics. The dynamic manifold intake is defined by the mass conservation theory and ideal air gas hypothesis in the following terms:

$$\dot{P}_{in} = \frac{RT_{in}}{v_{in}}\left(\dot{m}_{th} - \dot{m}_{Cyt}\right) + P_{in}\frac{\dot{T}_{in}}{T_{in}} \qquad (4)$$

$$\dot{P}_{in} = \Psi(\phi_{th}, P_{in}, T_{in}, N_e) \qquad (5)$$

Where, Pin shows manifold pressure, vin demonstrates the input volume, and Tin represents the input tempera- ture; the gas constant is R; fth illustrates the throttle opening position. The mass flow into cylinders is repre-sented as m_ Cyt; the mass flow through the valve is demonstrated as m_ th; and engine speed is Ne. The tem- perature is assumed to be constant. Thus, equation (4) becomes:

$$\dot{P}_{in} = \dot{k}_{in}\left(\dot{m}_{th} - \dot{m}_{Cyt}\right) \qquad (6)$$

$$with \quad \dot{k}_{in} = \frac{RT_{in}}{v_{in}} \qquad (7)$$

The mass flow through the valve is:

$$\dot{m}_{th} = C_d \frac{P_{id}}{\sqrt{RT_{id}}} S_{es}(\phi_{th})\; g\;(P_r) \qquad (8)$$

Cd the coefficient of discharge. The variable Pidillustrates the pressure due to overhead loading and the load ratio Pr is the overload pressure $P_r = \frac{P_{in}}{P_{id}}$. The feature Ses fð thÞ is the area of throttle opening. In an implementation, the product Cd Ses fð thÞ is considered and also known as a single feature of throttle valve opening. It is demonstrated in several different models. The one chosen in this work is:

$$S_{e\alpha}(\phi_{th}) = C_d \;\; S_{es}(\phi_{th}) = \sigma_1\{1 - \cos(\sigma_2\phi_{th} + \sigma_3)\} + \sigma_4 \qquad (9)$$

where s1=0:00051, s2=2:4357, s3=0:052, and s4=0:0011 are constants. The g(Pr) shows the nonlinear relationship as:

$$g\;(P_r) = \begin{cases} \sqrt{\frac{2\gamma}{\gamma-1}}(P_r)^{\frac{1}{\gamma}}\sqrt{\left(1 - P_r^{\frac{\gamma-1}{\gamma}}\right)} & if \quad P_r > \left(\frac{2}{\gamma+1}\right)^{\frac{\gamma}{\gamma-1}} \\ \sqrt{\gamma}\left(\frac{2}{\gamma+1}\right)^{\frac{\gamma+1}{2(\gamma-1)}} & if \quad P_r \leq \left(\frac{2}{\gamma+1}\right)^{\frac{\gamma}{\gamma-1}} \end{cases} \qquad (10)$$

ISSN PRINT 2319 1775 Online 2320 7876

 UGC CARE Listed (Group -I) Journal Volume 11 , Iss 8, Aug 2022

Fuel dynamics. It is represented as:

$$\begin{cases} \dot{m}_{ff}(t) = \frac{1}{\tau_f}\left(-\dot{m}_{ff}(t) + x\dot{m}_{fi}(t)\right) \\ \dot{m}_{fv} = (1-x)\dot{m}_{fi}(t) \\ \dot{m}_f(t) = \dot{m}_{fv}(t) + \dot{m}_{ff}(t) \end{cases} \quad (11)$$

Where m_ fiðtÞ represents the fuel flow injection ½kg=s, tf is the fuel vapor process, m_ fv is vapor fuel flow ½kg=s, m€ff ðtÞ shows liquid mass fuel flow ½kg=s, and m_ f ðtÞ shows fuel flow in the cylinders ½kg=s, , is a state vector.44 The second solution has been selected in our case:

$$\tau_f(N_e) = \sigma_5 N_e^{-\sigma_6} \quad (12)$$

$$\varkappa(N_e) = \sigma_7 + \sigma_8 N_e \quad (13)$$

Where s5, s6, s7, s8 are constant parameters. The injector model is given by a linear relationship between the mass fuel flows from the injectors. The air-fuel ratio is then obtained:

$$\lambda_{cyl} = \frac{\dot{m}_{cyl}(t)}{\lambda_s \dot{m}_f(t)} \quad (14)$$

00m_ cyl (t)00 is mass of cylinder, m_ f (t) is mass fuel flow into the cylinder, ‘‘lcyl’’ is AFR in the cylinder.

Sensor model. The lambda sensor model is represented as:

$$\dot{\lambda}(t) = -\frac{1}{\tau_\lambda}\lambda(t) + \frac{1}{\tau_\lambda}\lambda_{cyl}(t - \tau(N_e(t))) \quad (15)$$

where tl represents the time delay. The time delay t in terms of engine speed NeðtÞ is represented as:

$$\tau(N_e(t)) = \frac{60}{N_e(t)}\left(1 + \frac{1}{n_{cyl}}\right) \quad (16)$$

State-space representation. It is represented as:

$$\begin{cases} \dot{x}_1 = f_1(.)x_1(t) - f_2(.)u(t) \\ \dot{x}_2 = -\frac{1}{\tau_\lambda}\lambda(t) + \frac{1}{\tau_\lambda}\lambda_{cyl}(t - \tau(N_e(t))) \end{cases} \quad (17)$$

With $x_1(t) = \lambda_{cyl}$, $x_2(t) = \lambda(t)$, and $u(t) = \dot{m}_{fi}(t)$:

$$f_1(.) = -\frac{1}{\tau_\lambda(N_e)} - \frac{\dot{m}_{cyl}}{m_{cyl}(N_e, P_{in})} \quad (18)$$

$$f_2(.) = \lambda_s \frac{\chi(N_e)}{\tau_f(N_e)} m_{cyl}(N_e, P_{in}) \quad (19)$$

Here “$f_1(.)$” and “$f_2(.)$” are nonlinear functions that are bounded as follows: $\underline{f}_i \leq f_i(.) \leq \bar{f}_i$ *for* $i \in \{1, 2\}$.

Controller design

The controller design is adopted from Sui and Hall46 and given below:

$$y = u + \alpha x_1 + \beta x_2 \quad (20)$$

$$u = y_d + \alpha x_1 + \beta x_2 \quad (21)$$

Where the input is u, the output is y, and the esired output is yd, the state variables are x1 and x2, engine parameters are a and b, and finally Ne is engine speed. However, in this situation, we used predicted state observers,

$$u = y_d + \alpha \bar{x}_1 + \beta \bar{x}_2 \quad (22)$$

where x1 and x2 are the predicted values.

$$E = \frac{1}{2}(y - \bar{y})^2 \quad (23)$$

ISSN PRINT 2319 1775 Online 2320 7876

 UGC CARE Listed (Group -I) Journal Volume 11 , Iss 8, Aug 2022

Where the predicted output is y, the mean square error is E. The estimated output is represented as,

$$\bar{y} = u + \alpha\bar{x}_1 + \beta\bar{x}_2 \quad (24)$$

$$E = \frac{1}{2}(y - y_d)^2 \quad (25)$$

Equation (25) shows the mean square error function,so if we take the partial derivative of the previous equation,

$$\frac{\partial E}{\partial x_1} = -\alpha(y - y_d) \quad (26)$$

$$\frac{\partial E}{\partial x_2} = -\beta(y - y_d) \quad (27)$$

The gradient descent algorithm can change the state variables,

$$\bar{x}_1(k+1) = \bar{x}_1(k) - \eta\frac{\partial E}{\partial x_1} \quad (28)$$

$$\bar{x}_2(k+1) = \bar{x}_2(k) - \eta\frac{\partial E}{\partial x_2} \quad (29)$$

Where the estimated inputs are x1 and x2 are the predicted values. Adding equations (26) and (27) into the (28) and (29) we get,

$$\bar{x}_1(k+1) = \bar{x}_1(k) + \eta\alpha(y - y_d) \quad (30)$$

$$\bar{x}_2(k+1) = \bar{x}_2(k) + \eta\beta(y - y_d) \quad (31)$$

$$\therefore \eta = \frac{1}{\alpha^2 + \beta^2} \quad (32)$$

Add the value of h in the (30) and (31) equations,

$$\bar{x}_1(k+1) = \bar{x}_1(k) + \eta\frac{\alpha}{\alpha^2 + \beta^2}(y - y_d) \quad (32)$$

$$\bar{x}_2(k+1) = \bar{x}_2(k) + \eta\frac{\beta}{\alpha^2 + \beta^2}(y - y_d) \quad (33)$$

Lyapunov stability analysis is performed to check the system's stability. Let's assume the Lyapunov function is,

$$V(x(k)) = (y_d - y)^2 \quad (34)$$

Put the values of actual and desired outputs in equation (34),

$$V(x(k)) = [\alpha(x_1(k) - \bar{x}_1(k)) + \beta(x_2(k) - \bar{x}_2(k))] \quad (35)$$

The error estimation is,

$$\tilde{x}_1(k) = (x_1(k) - \bar{x}_1(k)) \quad (36)$$

$$\tilde{x}_2(k) = (x_2(k) - \bar{x}_2(k)) \quad (37)$$

So the Lyapunov function is,

$$V(x(k)) = [\alpha\tilde{x}_1(k) + \beta\tilde{x}_2(k)] \quad (38)$$

If we change ðkÞ cycle into ðk+1Þ the cycle then the equation is,

$$V(x(k+1)) = [\alpha\tilde{x}_1(k+1) + \beta\tilde{x}_2(k+1)] \quad (39)$$

Where,

$$\tilde{x}_1(k+1) = (x_1(k+1) - \bar{x}_1(k+1)) \quad (40)$$

$$\tilde{x}_2(k+1) = (x_2(k+1) - \bar{x}_2(k+1)) \quad (41)$$

Adding equations (32) and (33) into the (40) and (41) as follows,

ISSN PRINT 2319 1775 Online 2320 7876

 UGC CARE Listed (Group -I) Journal Volume 11 , Iss 8, Aug 2022

$$\bar{x}_1(k+1) = x_1(k+1) - \bar{x}_1(k) - \eta\frac{\alpha}{\alpha^2+\beta^2}(y-y_d) \quad (42)$$

$$\bar{x}_1(k+1) = x_2(k+1) - \bar{x}_2(k) - \eta\frac{\beta}{\alpha^2+\beta^2}(y-y_d) \quad (43)$$

Taking the difference between actual and predicted output is,

$$y - y_d = \alpha(x_1(k) - \bar{x}_1(k)) + \beta(x_2(k) - \bar{x}_2(k)) \quad (44)$$

$$y - y_d = \alpha\bar{x}_1(k) + \beta\bar{x}_2(k) \quad (45)$$

$$\bar{x}_1(k+1) = x_1(k+1) - \bar{x}_1(k) - \frac{\alpha}{\alpha^2+\beta^2}[\alpha\bar{x}_1(k) + \beta\bar{x}_2(k)] \quad (46)$$

$$\bar{x}_2(k+1) = x_2(k+1) - \bar{x}_2(k) - \frac{\beta}{\alpha^2+\beta^2}[\alpha\bar{x}_1(k) + \beta\bar{x}_2(k)] \quad (47)$$

$$x_1(k+1) = x_1(k) \quad (48)$$

$$x_2(k+1) = x_2(k) \quad (49)$$

$$\bar{x}_1(k+1) = x_1(k) - \bar{x}_1(k) - \frac{\alpha}{\alpha^2+\beta^2}[\alpha\bar{x}_1(k) + \beta\bar{x}_2(k)] \quad (50)$$

$$\bar{x}_2(k+1) = x_2(k) - \bar{x}_2(k) - \frac{\beta}{\alpha^2+\beta^2}[\alpha\bar{x}_1(k) + \beta\bar{x}_2(k)] \quad (51)$$

$$\bar{x}_1(k+1) = \bar{x}_1(k) - \frac{\alpha}{\alpha^2+\beta^2}[\alpha\bar{x}_1(k) + \beta\bar{x}_2(k)] \quad (52)$$

$$\bar{x}_2(k+1) = \bar{x}_2(k) - \frac{\beta}{\alpha^2+\beta^2}[\alpha\bar{x}_1(k) + \beta\bar{x}_2(k)] \quad (53)$$

The Lyapunov function can be written as,

$$V(x(k+1)) = \begin{bmatrix} \alpha\left[\bar{x}_1(k) - \frac{\alpha}{\alpha^2+\beta^2}[\alpha\bar{x}_1(k) + \beta\bar{x}_2(k)]\right] + \\ \beta\left[\bar{x}_2(k) - \frac{\beta}{\alpha^2+\beta^2}[\alpha\bar{x}_1(k) + \beta\bar{x}_2(k)]\right] \end{bmatrix} \quad (54)$$

$$V(x(k+1)) = 0 \quad (55)$$

So, the difference between both of them is,

$$V(x(k+1)) - V(x(k)) = -(y_d - y)^2 \quad (56)$$

$$V(x(k+1)) - V(x(k)) = -V(x(k)) \quad (57)$$

$$\therefore V(x(k)) = \dot{V}(x(k))$$

$$V(x(k+1)) - V(x(k)) = \dot{V}(x(k)) \quad (58)$$

The last equation shows that the difference between both cycles is negative definite and hence the Lyapunov stability proof is successfully achieved. The observer design with ANN was already discussed in Shahbaz and Amin4 for the AFTCS part. SMC mostly incorporates various control structure features and facilitates non-linear processes that are subject to large model uncertainties. SMC will form the passive part to react instantly to faults. Consider the MIMO system,

$$\dot{x}(t) = f(x) + \sum_{i=1}^{m} g_i(x)(u_i + F_i(x,t)) \quad (59)$$

$$y_i = h_i(x) \quad (60)$$

ISSN PRINT 2319 1775 Online 2320 7876

 UGC CARE Listed (Group -I) Journal Volume 11 , Iss 8, Aug 2022

Where u represents the input, x shows the state vector, and y is the output of the system. f ðxÞ and giðxÞ are vector fields, and hiðxÞ is a smooth function. Fiðx, TÞ demonstrates the uncertainty and it is further classified into structured and unstructured parts:

$$F_i(x,t) = \vartheta_{si} + \vartheta_{ui}(x,t) \qquad (61)$$

Where qsi is partial uncertainty and it is written as,

$$\vartheta_{si}(x) = \Delta_i \Xi_i(x) \qquad (62)$$

Consider sliding surface:

$$S_i = S_{oi}(x) + z_i \qquad (63)$$

Where S_i, $S_{oi}(x)$, and $z_i \in \mathbb{R}^m$. S_i is a sliding variable, and S_{oi} is a conventional sliding mode design. The structure of sliding surfaces is controlled by:

$$\dot{S}_i = \frac{\partial S_{oi}}{\partial x_i}\left[f_i(x) + \sum_{k=1}^{m} g_k(x)\{u_k + F_k(x,t)\}\right] + \dot{z}_i \qquad (64)$$

$$\dot{S}_i = \frac{\partial S_{oi}}{\partial x_i} f_i(x) + \frac{\partial S_{oi}}{\partial x_i}\sum_{k=1}^{m} g_k(x)\{u_k + F_k(x,t)\} + \dot{z}_i \qquad (65)$$

We can write as:

$$\dot{S} = N(x) + G(x)(U + F) + \dot{Z} \qquad (66)$$

Where $N(x) = \left[\frac{\partial S_{o1}}{\partial x_1} f_1(x), \ldots, \frac{\partial S_{om}}{\partial x_m} f_m(x)\right]^T$, $\dot{Z} = [\dot{z}_1, \ldots, \dot{z}_m]^T$, $G(x) = [G_1(x), \ldots, G_m(x)]^T$, and $G_i(x)(U+F) = \frac{\partial S_{oi}}{\partial x_i}$ $\sum_{k=1}^{m} g_k(x)\{u_k + F_k(x,t)\}$. Taking:

$$U = U_o + \bar{U} \qquad (67)$$

Where Uo maintain the known terms, and Uo manage the uncertain terms and actuators' faults. Assume that G1ðxÞ exists and taking Uo as:

$$U_o = G^{-1}(x)\{-N(x)\} \qquad (68)$$

Where Uo provides the desired output and eliminates all uncertainties and faults as well. Taking _Z as:

$$\dot{Z} = -N(x) - G(x)U_o \qquad (69)$$

The remaining system can be handled over:

$$\dot{S}_i = F_i + \bar{u}_i \qquad (70)$$

$$\dot{S}_i = \Delta_i \Xi_i(x) + \vartheta_{ui}(x,t) + \bar{u}_i \qquad (71)$$

Unstructured uncertainties are assumed to be handled as:

$$|\vartheta_{ui}(x,t)| \leq \Omega |S_i(x)|^{\frac{1}{2}} \qquad (72)$$

The controller structure ui is taken as:

ISSN PRINT 2319 1775 Online 2320 7876

Research paper **© 2012 IJFANS. All Rights Reserved,** UGC CARE Listed (Group -I) Journal Volume 11 , Iss 8, Aug 2022

$$\bar{u}_i = -M_i|S_i|^{\frac{1}{2}}\,sign(S_i) - \hat{\Delta}_i\Xi_i(x) \tag{73}$$

The Lyapunov function is used to get adaptation laws of unknown parameters (Δ_i):

$$V = \sum_{i=1}^{m}\left[|S_i| + \frac{1}{2\gamma_i}\hat{\Delta}_i^{\,2}\right] \tag{74}$$

Where $\gamma_i>0$. Consider now the time derivative of the Lyapunov function (74).

$$\dot{V} = \sum_{i=1}^{m}\left[sign(S_i)\dot{S}_i + \frac{1}{\gamma_i}\widetilde{\Delta}_i\dot{\hat{\Delta}}_i\right]\sum \tag{75}$$

Using equations (71) to (73) in (75).

$$\dot{V} = \sum_{i=1}^{m}\left[sign(S_i)\left\{\vartheta_{ud}(x,t) - M_i|S_i|^{\frac{1}{2}}sign(S_i) - \left(\hat{\Delta}_i - \Delta_i\right)\Xi_i(x)\right\} + \frac{1}{\gamma_i}\tilde{\Delta}_i\dot{\hat{\Delta}}_i\right] \tag{76}$$

$$\therefore\dot{V} = \sum_{i=1}^{m}\left[sign(S_i)\left\{\Omega_i|S_i|^{\frac{1}{2}} - M_i\,|S_i|^{\frac{1}{2}}\right\} + \tilde{\Delta}_i\left\{-sign(S_i)\Xi_i(x) + \frac{1}{\gamma_i}\dot{\hat{\Delta}}_i\right\}\right] \tag{77}$$

If $\hat{\Delta}_i s$ are exactly known, then $\tilde{\Delta}_i = 0$ and $\dot{V}$ becomes:

$$\dot{V} \leq \sum_{i=1}^{m}\left[|S_i|^{\frac{1}{2}}\,sign(S_i)\{\Omega_i - M_i sign(S_i)\}\right] \tag{78}$$

Selecting $M_i>\Omega_i$, $\dot{V}$ becomes negative. But $\hat{\Delta}_i s$ are not known perfectly, hence choosing the adaptation laws as:

$$\dot{\hat{\Delta}}_i = \gamma_i sign(S_i)\Xi_i(x) \tag{79}$$

We have:

$$\therefore\dot{V} \leq \sum_{i=1}^{m}\left[|S_i|^{\frac{1}{2}}\,sign(S_i)\{\Omega_i - M_i sign(S_i)\}\right] \tag{80}$$

Lyapunov stability analysis in equation (80) provides the best-estimated values of faults and does not require any constraints on structured disturbances.

The non-linear model of the IC engine described earlier provides the most important properties of the proposed controller. From the previous equation (4) of air dynamics, we can write as:

$$\dot{P}_{in} = \frac{RT_{in}}{v_{in}}\left(\dot{m}_{th} - \dot{m}_{Cyt}\right) + P_{in}\frac{\dot{T}_{in}}{T_{in}}$$

Where $k_{in} = \frac{RT_{in}}{v_{in}}$

$$\dot{P}_{in} = k_1\left(\dot{m}_{Cyt} - u_1 - P_{id}\right) \tag{81}$$

$$P_{id} = k_2\left(\dot{m}_{Cyt} - u_2 - u_1\right) \tag{82}$$

Where u1 and u2 is control inputs and k1 and k2 is mass flows. The output as set point regulation errors are selected as:

ISSN PRINT 2319 1775 Online 2320 7876

 UGC CARE Listed (Group -I) Journal Volume 11 , Iss 8, Aug 2022

$$y_1 = \dot{m}_{Cyt} - \dot{m}^d{}_{Cyt} \quad (83)$$

Where $\dot{m}^d{}_{Cyt}$ is the desired mass flow into the cylinder.

$$y_2 = \dot{P}_{id} - \dot{P}^d{}_{id} \quad (84)$$

Where $\dot{P}^d{}_{id}$ is desired overloading manifold pressure. Input-output linearization of output equations (83) and (84), put in equations (81) and (82) gives:

$$\dot{y}_1 = -\left(\frac{\dot{m}_{Cyt}}{\tau}\right) - a\left(\dot{m}_{Cyt} - k_{in}\dot{P}_{in}\right) + bu_2 - au_1 \quad (85)$$

$$\dot{y}_2 = k_2\left(k_{in}\dot{P}_{in} + \dot{m}^d{}_{Cyt}\right) - k_2u_1 - k_2u_2 \quad (86)$$

Control law:

The derivatives of the sliding variables after taking into account structured and unstructured uncertainties are:

$$\dot{S}_1 = -\left(\frac{\dot{m}_{Cyt}}{\tau}\right) - a\left(\dot{m}_{Cyt} - k_{in}\dot{P}_{in}\right) + bu_2 - au_1 - \Theta_1 - \vartheta u_1 + \dot{z}_1 \quad (87)$$

$$\dot{S}_2 = k_2\left(k_{in}\dot{P}_{in} + \dot{m}^d{}_{Cyt}\right) + k_2u_2 - k_2u_1 - \Theta_2 - \vartheta u_2 + \dot{z}_2 \quad (88)$$

Here, Yi represents the structured faults. These structured faults can be represented in terms of flow rates:

$$\Theta_1 = \Delta_1\Xi_1(x) = \Delta_1\dot{m}_{Cyt} \quad (89)$$

$$\Theta_2 = \Delta_2\Xi_2(x) = \Delta_2\dot{m}_{th} \quad (90)$$

Where Y1 and Y2 represents the over and under-flow through exhaust gas recirculation and variable geometry turbo actuators respectively. It is assumed that unstructured uncertainties are bounded:

$$|\vartheta_{u1}(x,t)| \leq \Omega_1|S_1(x)|^{\frac{1}{2}}, \quad \Omega_1 > 0 \quad (91)$$

$$|\vartheta_{u2}(x,t)| \leq \Omega_2|S_2(x)|^{\frac{1}{2}}, \quad \Omega_2 > 0 \quad (92)$$

The control action is proposed in equation (67). To work out uoi (control that can stabilize unaffected plant), ignoring structured faults, and unstructured faults in equations (85) and (86):

$$\dot{S}_{o1} = -\left(\frac{\dot{m}_{Cyt}}{\tau}\right) - a\left(\dot{m}_{Cyt} - k_{in}\dot{P}_{in}\right) + bu_2 - au_1 - \Theta_1 - \vartheta u_1 + \dot{z}_1 \quad (93)$$

ISSN PRINT 2319 1775 Online 2320 7876

Research paper **© 2012 IJFANS. All Rights Reserved,** UGC CARE Listed (Group -I) Journal Volume 11 , Iss 8, Aug 2022

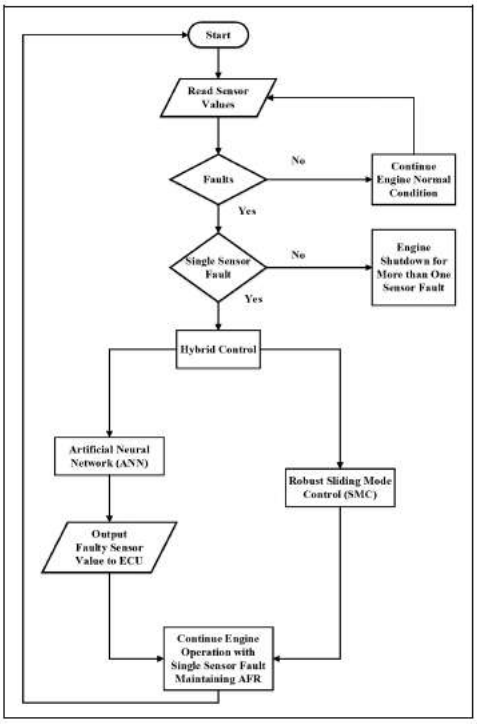

Figure 4. Proposed model of HFTCS.

$$\dot{S}_{o2} = k_2\left(k_{in}\dot{P}_{in} + \dot{m}^d{}_{Cyt}\right) + k_2u_2 - k_2u_1 - \Theta_2 - \vartheta u_2 + \dot{z}_2 \tag{94}$$

For ideal plant:

$$u_{o1} = \frac{1}{a+b}\left[-\dot{m}_{Cyt}\left(a + \frac{1}{\tau}\right) + (a+b)k_{in}\dot{P}_{in} + b\dot{m}^d{}_{Cyt}\right] \tag{95}$$

$$u_{o2} = \frac{1}{a+b}\left[-\dot{m}_{Cyt}\left(a + \frac{1}{\tau}\right) + b\dot{m}^d{}_{Cyt}\right] \tag{96}$$

3. RESULTS AND DISCUSSIONS

For fault detection, isolation, and reconfiguration of controllers, FDI is implemented in the model with ANN. The FDI unit continuously tracks the sensor values for any fault. If the sensor value exceeds the specified limit, a fault is detected by threshold comparison. Once the fault has been observed, an estimated value of the observer model based on ANN is substituted for the fault value and is supplied to the ECU. The active part performs post-fault optimal performance for the active compensation by providing the estimated value of the faulty sensor by ANN observer using the other healthy sensors. Two ANNs have been introduced for throttle and MAP sensors. Since the engine is running at 300 r/min, this value has been supplied to the controller if a fault occurs in the speed sensor. The AFTCS portion is simulated with sensor faults one at a time and the effects on the AFR are observed at t=5 s due to the internal warm-up delay of the engine, as shown in Figure 5. Results from Figure 5 show that the AFR is constantly degraded to 11.7 with

ISSN PRINT 2319 1775 Online 2320 7876

 UGC CARE Listed (Group -I) Journal Volume 11 , Iss 8, Aug 2022

every single sensor fault on the AFTCS portion alone. The passive part of the system consists of robust SMC. It provides a very quick response against fault, and after a very minor glitch in the output, the system maintains its steady state. Since the AFR decreases to 11.7 in the AFTCS part, the SMC controller with a fuel actuator is designed to keep it to 14.6 in faulty conditions.

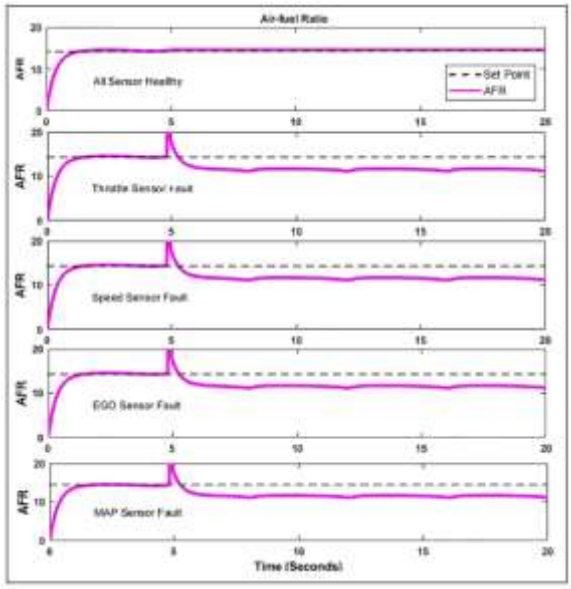

Figure 5. Performance of AFTCS.

In each of the four sensors, the faults are inserted at t=0 s, and the results on the AFR are detected at t=5 s due to internal warm-up times of 5 s in the original model. Figure 6 shows the results achieved for each sensor without noise in the sensors. The output response of the proposed PFTCS for faults in each sensor is demonstrated in Figure 6. In the existing model, AFR is affected by faults in each sensor and decreases to 11.7, that is, degradation in the performance in faulty conditions. However, the proposed PFTCS maintains AFR to 14.6 in normal as well as faulty conditions. These results show that the proposed PFTCS is robust to single-sensor faults. The performance of the overall HFTCS for the four sensors is shown in Figure 7 in normal and faulty conditions. The system maintains an AFR of 14.6 in faulty situations, according to the results. The proposed HFTCS is resistant to sensor faults, preserving its performance and thereby avoiding AFR degradation. The results represent that after a very minor glitch, the system maintains its steady state with the help of a robust SMC controller. Table 4 illustrates the robustness of

ISSN PRINT 2319 1775 Online 2320 7876

 UGC CARE Listed (Group -I) Journal Volume 11 , Iss 8, Aug 2022

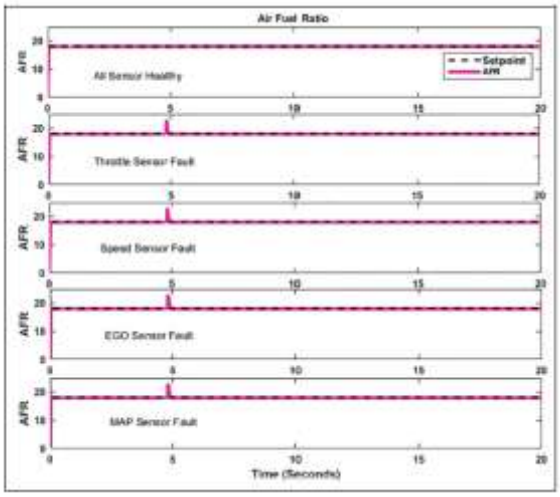

Figure 6. Performance of PFTCS.

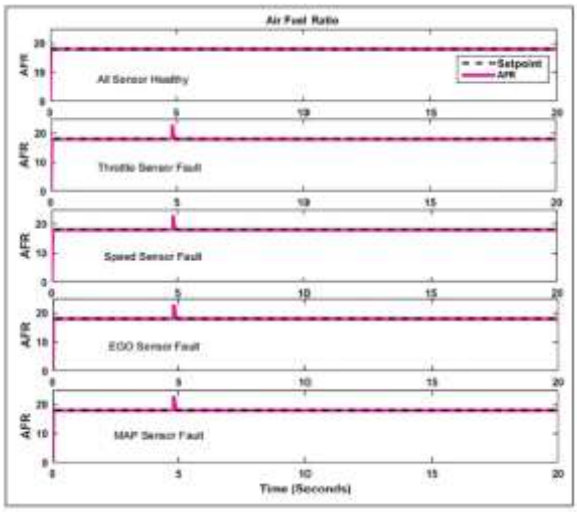

Figure 7. Performance of HFTCS without noise.

Table 4. Performance of Proposed HFTCS without noise introduced.

Faulty sensor	AFR	Stability issue
Throttle sensor	No effect on AFR	AFR is stable
Speed sensor	No effect on AFR	AFR is stable
MAP sensor	No effect on AFR	AFR is stable
EGO sensor	No effect on AFR	AFR is stable

Table 5. Parameters of noise for sensors.

Parameters of noise	MAP and EGO	Speed and throttle
Seed	[23341]	[23341]
Sampling time	0.1	0.1
Noise power	0.0001	0.01

the proposed HFTCS with ANN and SMC without noisy conditions of sensors. After confirming adequate efficiency in noise-free operation, the system response is tested by

ISSN PRINT 2319 1775 Online 2320 7876

Research paper **© 2012 IJFANS. All Rights Reserved,** UGC CARE Listed (Group -I) Journal Volume 11 , Iss 8, Aug 2022

integrating noise into sensor measurements. Table 5 shows the noise parameters introduced in the sensors. Greater noise is incorporated for throttle and speed sensor measurements due to high sensor values. Due to the very limited range, smaller noise is added in sensors EGO and MAP. In Figure 8, the effects of AFR are illustrated in normal and faulty conditions. The results demonstrated that after very minor sparks in the output, the system achieves the set point even under faulty conditions. The AFR remains stable with small misfires and the system continues to operate successfully in the noisy conditions of sensors. The performance of the proposed HFTCS with noise introduced is shown in Table 6. The output response in Figure 8 is dominated by the PFTCS that is running in parallel with AFTCS. The active part performs post-fault optimal performance for the active compensation by providing the estimated value of the faulty sensor by ANN observer using the other healthy sensors. Since both controllers work in parallel, the active compensation effect does not become much evident due to the dominance of the passive controller. However, it becomes very much evident in only active FTCS as shown in Figure 5.

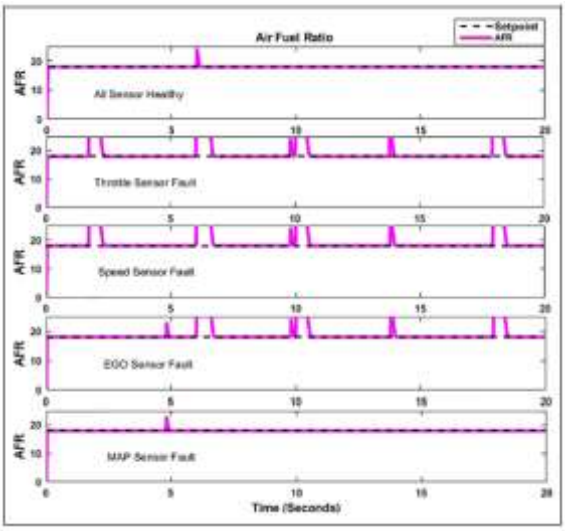

Figure 8. Performance of HFTCS in noisy conditions.

Table 6. Performance of Proposed HFTCS with noise introduced.

Faulty sensor	AFR	Stability issue
Throttle sensor	No effect on AFR	AFR is stable
Speed sensor	No effect on AFR	AFR is stable
MAP sensor	No effect on AFR	AFR is stable
EGO sensor	No effect on AFR	AFR is stable

Comparison with the existing works

In this section, a comparison of the proposed HFTCS with the existing models is discussed. We have designed an HFTCS with dedicated non-linear controllers known as ANN and SMC. The previous work has not used the ANN and SMC together for HFTCS design for the AFR system of the IC Engine. In the proposed system, SMC will form the passive part to

ISSN PRINT 2319 1775 Online 2320 7876

 UGC CARE Listed (Group -I) Journal Volume 11 , Iss 8, Aug 2022

react instantly to faults while ANN will optimize post-fault performance with active compensation. Moreover, Lyapunov stability analysis was performed to make sure that the system remains stable in both normal and faulty conditions. The estimated values of the throttle and MAP sensors, as well as the accompanying mean square errors (MSE), are shown in Shahbaz and Amin.4 ANN approach can cover the complete nonlinear range of the MAP sensor, which is also less computationally expensive than lookup tables and hence preferred. Due to its valuable functionalities of learning, self-organization, and non-linear modeling capabilities, the ANN technique is currently becoming a preferred strategy in fault diagnostics. In Amin and Mahmood-ul-Hasan,14 the HFTCS was proposed with Kalman Filters in the active part and a high-gain PI controller in the passive part. This algorithm was limited to the linear range of the highly nonlinear sensors of the AFR control system. In Su et al.,15 the HFTCS was proposed for the sensors of the distillation column without using any intelligent control or data-driven technique. In Wang et al.,16 the HFTCS was proposed for the uncertain networked control systems under a discrete event-triggered communication scheme that was not applied to the process plant. In Yang et al.,48 the authors focused on faulttolerant control of Markov jump systems (MJS) with Itoˆ stochastic process and output disturbances. A proportional-derivative sliding mode observer (SMO) and an observer-based controller are first devised and fabricated. In Yang et al.,49 the authors provided a fault-tolerant compensation control strategy for Markov jump systems against nonlinearity, simultaneous additive, and multiplicative actuator failures. A fuzzy logic system (FLS) was used to estimate the nonlinear functions and by using the adaptive backstepping approach, an FLS-based adaptive fault-tolerant compensation controller is developed. The proposed methods worked very well for the stochastic disturbances and simultaneous additive and multiplicative type faults in the actuators. However, the stochastic delays and actuator faults were not studied in this paper. The proposed HFTCS has PFTCS for AFR control, which is based on SMC, and AFTCS based on ANN. With the use of a fuel throttle actuator, the proposed HFTCS will compensate for the AFR degradation by the AFR control. In the proposed system, SMC will form the passive part to react instantly to faults while ANN will optimize post-fault performance with active compensation as shown in Figure 5. The previous works mentioned in the literature have not yet utilized any intelligent control technique like ANN for the AFTCS and regular sliding mode control for the PFTCS, as proposed in this paper. The proposed model was found to be robust to faults in the normal and noisy conditions of the sensors. Therefore, the proposed HFTCS with ANN and SMC presents an optimum and reliable solution for AFR control in SI IC engines. Table 7 provides a comprehensive comparison of the suggested strategy with previously used strategies.

Table 7. Comparison of proposed HFTCS with previous works.[43,50–53]

Name of controller	Major drawback	Chattering reduction	Degree of robustness	Response against noise
Proposed HFTCS	Misfires	Can be further improved with advanced SMC	High	Relatively low misfiring observed
HFTCS based on Kalman filter	Linear range of sensors	Does not eliminate chattering	Moderate	High misfiring observed
HFTCS based on GA and HOSMC	Oscillations in AFR transient response	Better	High	High misfiring observed
HFTCS based on FLC and HOSMC	Oscillations in AFR transient response	Better	High	High misfiring observed
AFTCS based on ANN and FLC	Performance degradation	Does not eliminate chattering	Unknown duration for handling faults	High misfiring observed
AFTCS based on non-linear regression	Performance degradation	Does not eliminate chattering	Not a robust technique	High misfiring observed

ISSN PRINT 2319 1775 Online 2320 7876

 UGC CARE Listed (Group -I) Journal Volume 11 , Iss 8, Aug 2022

4. CONCLUSIONS

In this paper, a novel HFTCS was proposed for the AFR control of the IC engine based on the advanced non-linear controllers: ANN and SMC. With the use of a fuel throttle actuator, the proposed HFTCS was able to compensate for the AFR degradation with SMC that formed the passive part to react instantly to faults while ANN was able to optimize post-fault performance with active compensation. The Lyapunov stability analysis was also performed to make sure that the system remains stable in both normal and faulty conditions. The fault tolerance was checked with noisy measurements of sensors to examine the robustness of the proposed controller. The simulation results in the Matlab/Simulink environment show that the designed controller is robust to faults in normal and noisy measurements of the sensors and reliable. Furthermore, a comparison with the existing works was also carried out to demonstrate its superior performance. Future works may include the design of HFTCS with modern control techniques known as Deep learning with Adaptive SMC, Neuro-Fuzzy SMC, and Integral SMC by testing at higher speeds considering load variations. Partial faults may also be considered with these techniques with experimental verification using the hardware-in-the-loop technique. Another direction is to consider the stochastic delays for the fault-tolerant AFR controller design. Acknowledgement The authors would like to thank colleagues for suggestions to improve paper quality. Declaration of conflicting interests The author(s) declared no potential conflicts of interest with respect to the research, authorship, and/or publication of this article.

Funding
The author(s) received no financial support for the research, authorship, and/or publication of this article.

5. REFERENCES

1. Jiang J. Fault-tolerant control Systems: an introductory overview1. Zidonghua Xuebao 2005; 31: 14.
2. Frank PM. Trends in fault-tolerant control of engineer- ing systems. IFAC Proc Volumes 2004; 37: 377–384.
3. Amin AA and Hasan KM. A review of fault tolerant control systems: advancements and applications. Mea- surement 2019; 143: 58–68.
4. Shahbaz MH and Amin AA. Design of active fault toler- ant control system for air fuel ratio control of internal combustion engines using artificial neural networks. IEEE Access 2021; 9: 46022–46032.
5. Amin AA and Mahmood-ul-Hasan K. Robust active fault-tolerant control for internal combustion gas engine for air–fuel ratio control with statistical regression-based observer model. Meas Control 2019; 52: 1179–1194.
6. Jiang J and Yu X. Fault-tolerant control systems: A comparative study between active and passive approaches. Annu Rev Control 2012; 36: 60–72.
7. Mahmoud M and Xia Y. Industrial fault-tolerant archi- tectures. In: Analysis and synthesis of fault-tolerant con- trol systems. Chichester: John Wiley & Sons, Ltd, 2013, 307–319.

ISSN PRINT 2319 1775 Online 2320 7876

 UGC CARE Listed (Group -I) Journal Volume 11 , Iss 8, Aug 2022

8. Ahmed S, Amin AA, Wajid Z, et al. Reliable speed control of a permanent magnet DC motor using fault-tolerant H-bridge. Adv Mech Eng 2020; 12: 1687814020970311.
9. Benosman M. Passive fault tolerant control. Cambridge: IntechOpen, 2011.
10. Amin AA and Mahmood-Ul-Hasan K. Advanced Fault Tolerant Air-fuel ratio control of internal combustion gas engine for sensor and actuator faults. IEEE Access 2019; 7: 17634–17643.
11. Amin AA and Mahmood-ul-Hasan K. Robust passive fault tolerant control for air fuel ratio control of internal combustion gasoline engine for sensor and actuator faults. IETE J Res 2021; 1–16.
12. Blanke M, Staroswiecki M and Wu NE. Concepts and methods in fault-tolerant control. In: Proceedings of the 2001 American Control Conference (cat. no. 01CH37148), Arlington, VA, USA, 2001, vol. 4, pp.2606–2620.
13. Yuan Y, Liu X, Ding S, et al. Fault detection and loca- tion system for diagnosis of multiple faults in aeroen- gines. IEEE Access 2017; 5: 17671–17677.
14. Amin AA and Mahmood-ul-Hasan K. Hybrid fault toler- ant control for air–fuel ratio control of internal combus- tion gasoline engine using Kalman filters with advanced redundancy. Meas Control 2019; 52: 473–492.
15. Su SW, Bao J and Lee PL. A hybrid active–passive fault- tolerant control approach. Asia Pac J Chem Eng 2006; 1: 54–62.
16. Wang J, Yao X and Li W. Hybrid active-passive robust fault-tolerant control of event-triggered nonlinear NCS. Open Electr Electron Eng J 2017; 11: 68–86.
17. Li L. Fault detection and fault-tolerant control for non- linear systems. Wiesbaden: Springer Fachmedien Wiesba- den, 2016.
18. Yang H, Jiang B and Cocquempot V. Fault tolerant con- trol design for hybrid systems, vol. 397. Berlin, Heidelberg: Springer Berlin Heidelberg, 2010..
19. Tang L, Ma D and Zhao J. Neural networks-based active fault-tolerant control for a class of switched nonlinear sys- tems with its application to RCL circuit. IEEE Trans Syst Man Cybern 2018; 50: 4270–4282. https://ieeexplore.ieee. org/document/8409459
20. Patel HR and Shah V. Fuzzy logic based passive fault tolerant control strategy for a single-tank system with system fault and process disturbances. In: 2018 5th inter- national conference on electrical and electronic engineering (ICEEE), Istanbul, Turkey, 2018, pp.257–262.
21. Murtaza G, Bhatti AI and Butt YA. Super twisting controller-based unified FDI and FTC scheme for air path of diesel engine using the certainty equivalence prin- ciple. Proc IMechE, Part D: J Automobile Engineering 2018; 232: 1623–1633.
22. Pourbabaee B, Meskin N and Khorasani K. Sensor fault detection, isolation, and identification using multiple- model-based hybrid Kalman filter for gas turbine engines. IEEE Trans Control Syst Technol 2015; 24: 1184–1200.
23. Amin AA and Mahmood-ul-Hasan K. Unified fault- tolerant control for air-fuel ratio control of internal com- bustion engines with advanced analytical and hardware redundancies. J Electr Eng Technol 2022; 17: 1947–1959.
24. Bum E and Wilczek F. Supervised learning of probability distributions by neural networks. In: Neural information processing systems, New Orleans, LA, 1988. Available at: https://proceedings.neurips.cc/paper/1987/file/eccbc87e4b 5ce2fe28308fd9f2a7baf3-Paper.pdf (accessed 18 February 2021).

ISSN PRINT 2319 1775 Online 2320 7876

 UGC CARE Listed (Group -I) Journal Volume 11 , Iss 8, Aug 2022

25. Vinnakoti S and Kota VR. Implementation of artificial neural network based controller for a five-level converter based UPQC. Alex Eng J 2018; 57: 1475–1488.
26. Hagan MT, Demuth HB and Jesu´s OD. An introduction to the use of neural networks in control systems. Int J Robust Nonlinear Control 2002; 12: 959–985.
27. De Jesus O, Pukrittayakamee A and Hagan M. A com- parison of neural network control algorithms. In: IJCNN'01: International joint conference on neural net- works. Proceedings (cat. no. 01CH37222), Washington, DC, USA. Available at: https://www.semanticscholar. org/paper/A-comparison-of-neural-network-control-algori thms-Jesus-Pukrittayakamee/abb298be32d077f42f71177d44 3bfef332e9c1b1 (accessed 18 May 2021).
28. Abu-Mahfouz IA. A comparative study of three artificial neural networks for the detection and classification of gear faults. Int J Gen Syst 2005; 34: 261–277.
29. Arabacı H and Bilgin O. Automatic detection and classi- fication of rotor cage faults in squirrel cage induction motor. Neural Comput Appl 2010; 19: 713–723.
30. Gao H, Song Y and Wen C. Backstepping design of adaptive neural fault-tolerant control for MIMO non- linear systems. IEEE Trans Neural Netw Learn Syst 2017; 28: 2605–2613.
31. Wang Y, Zhang M, Wilson PA, et al. Adaptive neural network-based backstepping fault tolerant control for underwater vehicles with thruster fault. Ocean Eng 2015; 110: 15–24.
32. Yin S, Yang H, Gao H, et al. An adaptive NN-based approach for fault-tolerant control of nonlinear time-varying delay systems with unmodeled dynamics. IEEE Trans Neural Netw Learn Syst 2017; 28: 1902–1913.
33. Incremona GP, Rubagotti M and Ferrara A. Sliding mode control of constrained nonlinear systems. IEEE Trans Automat Contr 2017; 62: 2965–2972.
34. Nemati H, Bando M and Hokamoto S. Chattering attenuation sliding mode approach for nonlinear systems. Asian J Control 2017; 19: 1519–1531.
35. Murtaza G, Bhatti AI and Butt YA. Unified FDI and FTC scheme for Air Path actuators of a diesel engine using ISM extended with adaptive part. Asian J Control
2020; 22: 117–129.
36. Du C and Xing G. Control of nonlinear distributed para- meter systems based on global approximation. J Appl Math 2014; 2014: 1–6.
37. Riaz U, Tayyeb M and Amin AA. A review of sliding mode control with the perspective of utilization in fault tolerant control. Recent Adv Electr Electr Eng 2021; 14: 312–324
38. Utkin VL, Chang H-C, Kolmanovsky I, et al. Sliding mode control for variable geometry turbocharged diesel engines. In: Proceedings of the 2000 American control con- ference. ACC (IEEE cat. no. 00CH36334), Chicago, IL, USA, 2000, vol. 1, no. 6, pp.584–588.
39. Applications | Gas Engine Controls. Available at: http:// www.gasenginecontrols.com/applications/ (accessed 18 April 2021).
40. Lauber J, Khiar D and Guerra TM. Air-fuel ratio control for an ic engine. In: 2007 IEEE vehicle power and propul- sion conference, Arlington, TX, USA, 2007, pp. 718–723.
41. Modeling a fault-tolerant fuel control system – MATLAB & Simulink. Available at: https://www.mathworks.com/ help/simulink/slref/modeling-a-fault-tolerant-fuel-

ISSN PRINT 2319 1775 Online 2320 7876

 UGC CARE Listed (Group -I) Journal Volume 11 , Iss 8, Aug 2022

control- system.html;jsessionid=6068d2d9cdc5c26e2c47bd6c6df1 (accessed 29 July 2022).
42. Modeling engine timing using triggered subsystems – MATLAB & Simulink. Available at: https://www.ma thworks.com/help/simulink/slref/modeling-engine-timing-using-triggered-subsystems.html (accessed 29 July 2022).
43. Crossley PR and Cook JA. A nonlinear engine model for drivetrain system development. In: International confer- ence on control 1991. Control'91, Edinburgh, UK, 1991, pp.921–925.
44. Hendricks E and Sorenson SC. Mean value modelling of spark ignition engines. SAE Trans 1990; 1359–1373.
45. Na J, Chen AS, Huang Y, et al. Air–Fuel ratio control of spark ignition engines with unknown system dynamics estimator: theory and experiments. IEEE Trans Control Syst Technol 2019; 29: 786–793.
46. Sui W and Hall CM. Combustion phasing modeling and control for compression ignition engines with high dilu- tion and boost levels. Proc IMechE, Part D: J Automobile Engineering 2019; 233: 1834–1850.
47. Hu K-Y, Li W and Cheng Z. Hybrid adaptive fault- tolerant control for compound faults of hypersonic vehi- cle. IEEE Access 2021; 9: 56927–56939.
48. Yang H, Jiang Y and Yin S. Fault-tolerant control of time-delay Markov jump systems with Itoˆstochastic pro- cess and output disturbance based on sliding mode obser- ver. IEEE Trans Ind Inform 2018; 14: 5299–5307.
49. Yang H, Jiang Y and Yin S. Adaptive fuzzy fault-tolerant control for Markov jump systems with additive and mul- tiplicative actuator faults. IEEE Trans Fuzzy Syst 2021; 29: 772–785.
50. Alsuwian T, Tayyeb M, Amin AA, et al. Design of a hybrid fault-tolerant control system for air–fuel ratio control of internal combustion engines using genetic algo-rithm and higher-order sliding mode control. Energies 2022; 15: 5666.
51. Alsuwian T, Riaz U, Amin AA, et al. Hybrid fault- tolerant control for air-fuel ratio control system of internal combustion engine using fuzzy logic and super- twisting sliding mode control techniques. Energies 2022; 15: 7010.
52. Riaz U, Amin AA and Tayyeb M. Design of active fault- tolerant control system for air-fuel ratio control of internal combustion engines using fuzzy logic controller. Sci Prog 2022; 105: 368504221094723.
53. Alsuwian T, Amin AA, Iqbal MS, et al. Design of active fault-tolerant control system for Air-Fuel ratio control of internal combustion engine using nonlinear regression-based observer model. PLoS One 2022; 17: e0279101.